Probing by Time-Resolved FTIR Spectroscopy Mass Transport, Molecular Interactions, and Conformational Ordering in the System Chloroform−Syndiotactic Polystyrene

P. Musto,*,† G. Mensitieri,‡ S. Cotugno,‡ G. Guerra,§ and V. Venditto§

Institute of Research and Technology of Plastic Materials, National Research Council of Italy, via Campi Flegrei 34, 80078, Pozzuoli (NA), Italy; Department of Materials and Production Engineering, University of Naples Federico II, Piazzale Tecchio 80, 80125, Naples, Italy; and Department of Chemistry, University of Salerno, 84081, Baronissi (SA), Italy

Received September 26, 2001; Revised Manuscript Received December 3, 2001

ABSTRACT: The transport of chloroform in films of semicrystalline syndiotactic polystyrene (s-PS) in its nanoporous form (δ-form) has been investigated by gravimetric analysis and time-resolved FTIR spectroscopy. Experimental tests have been performed at 56 °C and at several vapor pressures ranging from 5 to 100 Torr. Sorption and desorption kinetics have been monitored with both techniques, and the dependence of diffusion coefficients with penetrant concentration was investigated, evidencing Fickian features typical of systems characterized by diffusivity increasing with concentration. Analysis of the vibrational spectrum of chloroform sorbed in the crystalline phase showed significant perturbations when compared to the spectrum of the isolated molecule or the molecule absorbed in amorphous s-PS. This perturbation has been attributed to host−guest molecular interactions whose strength was found to be relatively small. Conformational rearrangements of macromolecular chains in the amorphous phase were detected as a consequence of chloroform sorption. These rearrangements, which lead to an increase of the overall crystallinity degree, were quantified using the concept of critical sequence length (CSL). The kinetics of the conformational ordering process was found to parallel the sorption kinetics, and the associated increase of crystallinity was not reversible upon chloroform desorption.

1. Introduction

Syndiotactic polystyrene (s-PS) is characterized by an elevated melting point (260 °C) and a high crystallization rate. Several structural studies have revealed a complex polymorphic behavior.[1−4] The various crystalline modifications differ with respect to the chain conformation as well as for the chain packing within the unit cell. Referring to the nomenclature proposed in the literature,[3] four main crystalline forms may be distinguished, denoted α, β, γ, and δ. The first two, α[5−7] and β,[1,8] have the chains in the trans-planar, zigzag conformation with identity period 5.1 Å, while the γ and δ[9] show a helical *s*(2/1)2 conformation of the chain with identity period of 7.7 Å. Clathrate structures where *s*(2/1)2 helices include several guest molecules have also been described.[10−12]

Treatments by different volatile organic compounds (mainly halogenated or aromatic hydrocarbons) not only can induce crystallization of amorphous samples but can also transform α and γ crystalline forms into clathrate forms; only for the β structure are these low molecular mass compounds selectively absorbed in the amorphous phase, while leaving the crystalline phase unaltered.[13] This is possibly related to the higher density of this crystalline form (1.078 g/cm^3) with respect to the others.

It has been recently found that, by using suitable extraction procedures,[14,15] guest molecules can be removed from the clathrate forms to obtain a nanoporous δ-form whose crystalline structure has been recently described.[9] The structure of this nanoporous crystalline form of s-PS is reported in Figure 1, where the dashed area represents the volume of the nanocavities present in the crystalline cell as probed by a hard sphere with a 1.8 Å radius: the volume of these cavities has been evaluated to be about 120 Å^3.[16] The nanoporous δ form readily produces clathrates when contacted with proper compounds; this process occurs at much lower activities than in the case of α or γ forms.[17,18]

In general, polymeric clathrates are more complex than those formed by low molecular mass hosts, since the former generally contain large amorphous fractions (typically around 50%). As a consequence, guest molecules can be included in both clathrate and amorphous phases.

The high sorption capacity of the crystalline phase makes this system very relevant from a scientific point of view. To our knowledge, this is the only case in which the crystalline polymer phase, normally impervious to low molecular weight compounds,[19] can absorb considerable amounts of penetrants, also for very low activities where sorption in the amorphous phase is negligible. It is worth noting, in this respect, that, in the case of isotactic poly(4-methylpentene) the penetrant sorption also involves the crystalline phase, but both diffusivity and solubility are smaller than for the amorphous phase.[20,21]

It is likely that, within the cavities of the crystalline phase, host−guest molecular interactions are established. This has been demonstrated by a FTIR spectroscopy investigation[22,23] and by molecular mechanics calculations[18] for the case of dichloroethane and dichloropropane.

A previous investigation of chloroform vapor sorption at 35 °C, in the range of activity 0.015−1, for s-PS samples in different crystalline forms,[17] evidenced the

† National Research Council of Italy.
‡ University of Naples Federico II.
§ University of Salerno.
* Corresponding author: e-mail musto@irtemp.na.cnr.it.

10.1021/ma011684d CCC: $22.00
Published on Web 02/07/2002

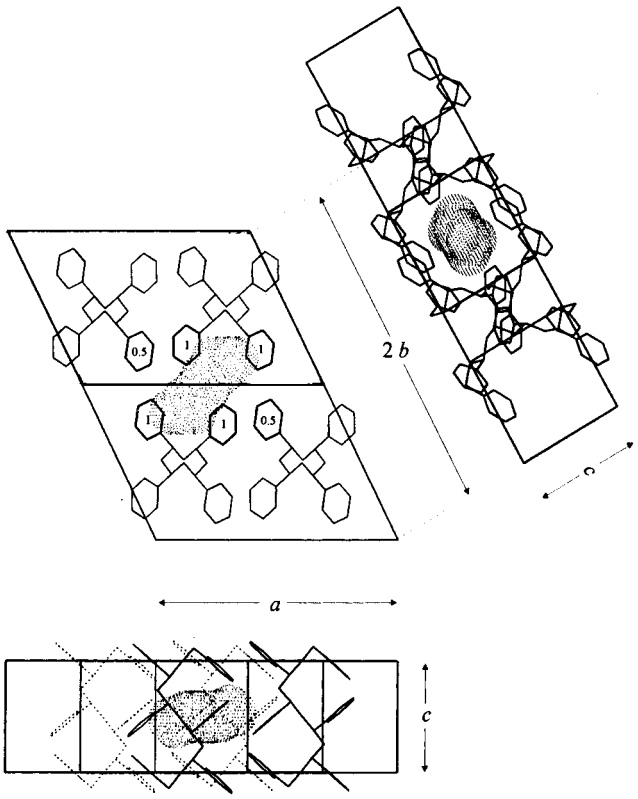

Figure 1. Molecular chain conformations in the crystalline δ form of s-PS.

high sorption capacity of the nanoporous form, even at very low vapor activities. These large equilibrium uptakes have been associated with clathration phenomena.

In the present contribution, chloroform transport in nanoporous s-PS is further investigated by means of gravimetric measurements and a recently developed spectroscopic technique based on in situ, time-resolved FTIR measurements.[24] The latter technique, besides providing a means for the accurate evaluation of transport kinetics, gives also the possibility of investigating molecular interactions formed between the penetrant and the polymer matrix as well as structural changes of the polymeric substrate which may result from the penetrant diffusion. These aspects will be discussed in detail in the present contribution.

2. Materials and Methods

2.1. Materials. s-PS was synthesized using a homogeneous catalyst consisting of $CpTiCl_3$ and methylalumoxane (MAO) in toluene, according to the method described in the literature.[25] The polymer fraction insoluble in acetone was 92%. The intrinsic viscosity of the acetone insoluble fraction, determined in tetrahydronaphthalene at 135 °C with an Ubbelhode viscometer, was 0.6 dL/g.

Film samples of δ form were obtained by a spin-coating procedure from 5 wt % solutions of s-PS in chloroform followed by treatment with boiling acetone for 5 h and desiccation at 60 °C for 2 h to remove chloroform. These samples were used to perform gravimetric measurements as well as in situ FTIR spectroscopy measurements during chloroform sorption. Typical film thicknesses in the range 8−15 μm where obtained by 10 successive depositions. Scanning electron microscopy was used for the accurate determination of film thickness.

2.2. Monitoring of Chloroform Sorption by in Situ Time-Resolved FTIR Spectroscopy. A vacuum-tight FTIR cell has been specifically constructed[24] to measure in situ the

Scheme 1. Apparatus for the in Situ FTIR Measurement of Mass Transport

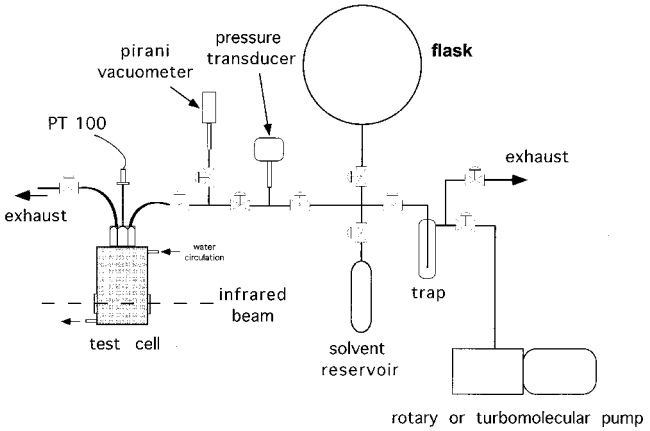

FTIR transmission spectrum of polymer films exposed to penetrant vapor at a controlled temperature and pressure (see Scheme 1). The cell can also be evacuated down to 10^{-3} Torr to monitor desorption processes.

Chloroform vapor sorption experiments were carried out on s-PS nanoporous films at four pressure values (5, 10, 20, and 100 Torr) at 56 °C. Each sorption run was performed on a different sample after prolonged exposure to vacuum (0.001 Torr) at 56 °C. The instrument used to collect spectra was a Perkin-Elmer System 2000 spectrometer equipped with a germanium/KBr beam splitter and a wide-band DTGS detector. The instrumental parameters adopted for the spectral collection were as follows: resolution = 4 cm^{-1}, optical path difference (OPD) velocity = 0.2 cm/s, spectral range 4000−400 cm^{-1}. A single data collection was performed for each spectrum (3601 data points) which, in the selected instrumental conditions, took 6 s to complete. It was found that, even with a single acquisition, the signal-to-noise ratio of the spectra (5000:1) was suitable for quantitative analysis. The signal was acquired as single beam at specific time intervals which increased as the process approached equilibrium.

A typical sorption run lasted up to 1 week, and acquisition time intervals were 30 s during the first 15 min of the experiment, afterward increasing gradually up to 30 min. Single beam spectra were processed to obtain the absorbance spectra, using as background the cell without the s-PS sample and filled only with pure chloroform vapor at exactly the same pressure at which sorption tests were performed. After the attainment of apparent sorption equilibrium, a desorption stage followed: the cell at the fixed chloroform vapor activity was first isolated from the rest of the apparatus, which was then put under vacuum; when an absolute pressure lower than 0.001 Torr was reached, the connection with cell was open and acquisition started. The desorption was monitored until the disappearance of the chloroform peaks. The background spectrum was that of the evacuated empty cell.

Pressure of chloroform vapor was measured by means of a pressure transducer Baraton 121, MKS Instruments, with a full scale of 10 or 100 Torr (resolution, 1×10^{-3} and 1×10^{-2} Torr; accuracy 0.5% of the readout). Isolation of the chloroform peak in the region 1230−1200 cm^{-1} was obtained by subtraction spectroscopy,[26,27] i.e.

$$A_d = A_s - KA_r \quad (1)$$

where A_d is the difference spectrum characteristic of absorbed chloroform, A_s is the spectrum of the chloroform containing sample, and A_r represents the spectrum of the starting (empty) sample. K is an adjustable parameter used to compensate for thickness differences between the sample and reference spectra. In the present case, since no thickness changes occurred upon chloroform sorption, K is consistently equal to unity. The same subtraction technique was employed to isolate the spectrum of ordered regions within the semicrystalline δ form.

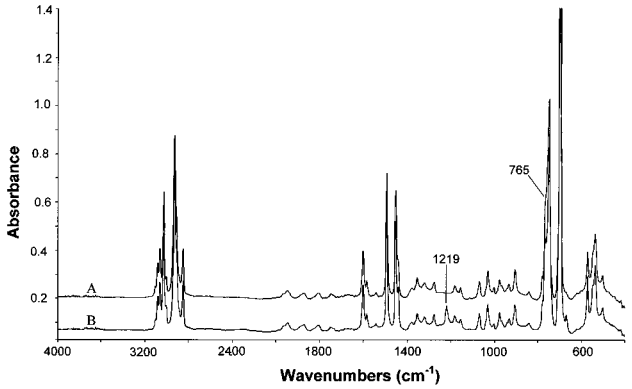

Figure 2. Transmission FTIR spectra in the 4000−400 cm^{-1} interval of a film of s-PS in δ form subjected to chloroform sorption at 56 °C and at 100 Torr: trace A, starting s-PS sample; trace B, sample after equilibration.

In this case, the spectrum of a fully amorphous s-PS film was taken as reference.

To separate the individual peaks in the case of unresolved, multicomponent bands, a curve-resolving algorithm was applied, based on the Levenberg−Marquardt method;[28] to reduce the number of adjustable parameters and to ensure the uniqueness of the result, the baseline, the band shape, and the number of components were fixed. The program was then allowed to calculate, by a nonlinear curve fitting of the data, the height, the full width at half-height (fwhh), and the position of the individual components.

The peak function was a mixed Gauss−Lorentz line shape of the form

$$f(x) = (1 - L)H \exp\left[-\left(\frac{x - x_0}{w}\right)^2 (4 \ln 2)\right] + L \frac{H}{4\left(\frac{x - x_0}{w}\right)^2 + 1} \quad (2)$$

where x_0 is the peak position, H the peak height, w the fwhh, and L the fraction of Lorentz character.

2.3. Gravimetric Analysis. The equipment used to determine weight gain of samples exposed to a chloroform vapor have been already described in a previous contribution.[24] It is similar to the apparatus reported in Scheme 1, with a controlled atmosphere electronic microbalance (CAHN D200, sensitivity equal to 0.1 μg) in place of the infrared cell.

3. Results and Discussion

3.1. Analysis of Mass Transport. The FTIR spectrum of an s-PS film in the empty δ-form is reported in Figure 2, trace A. Sorption of chloroform molecules induces significant modification of this spectrum, due to the contribution of the penetrant and to rearrangement of the s-PS crystalline structure. These features are evident in Figure 2, trace B, where is reported the spectrum of the same s-PS film after equilibration with chloroform vapor at 100 Torr and 56 °C. Chloroform peaks emerge at 1219 cm^{-1} (δ_{H-C-Cl}) and at 765 cm^{-1} (ν_{C-Cl}); changes in the area of the components are detected in the conformationally sensitive region between 600 and 450 cm^{-1}. The chloroform peak at 1219 cm^{-1} is fully resolved and reasonably free from interference of the polymeric substrate, thus representing an ideal candidate to evaluate the penetrant concentration.

Gradual development of the peak as the sorption proceeds is shown in Figure 3, relative to a test performed at 10 Torr and 56 °C. It is worth noting that the peak clearly shows a fine structure in the form of an unresolved component at a lower wavenumber (≅1210 cm^{-1}). This feature is not present in the spectrum of the isolated molecule (vapor phase) and in the case of chloroform sorbed in the amorphous phase of s-PS. Sorption kinetics can be evaluated from the absorbance area of the analytical peak in the spectra as a function of time (t). In the following, sorption and desorption kinetic curves are reported in normalized form, i.e., as $A_t/A_\infty = M_t/M_\infty$ for sorption and as $[A_0 - A(t)]/A_0 \equiv [M_0 - M(t)]/M_0$ for desorption, vs $t^{1/2}$/(sample thickness). The subscripts t, ∞, and 0 refer to mass (M) or absorbance (A) evaluated at time t and at sorption equilibrium (∞ for the sorption test, 0 for the desorption test).

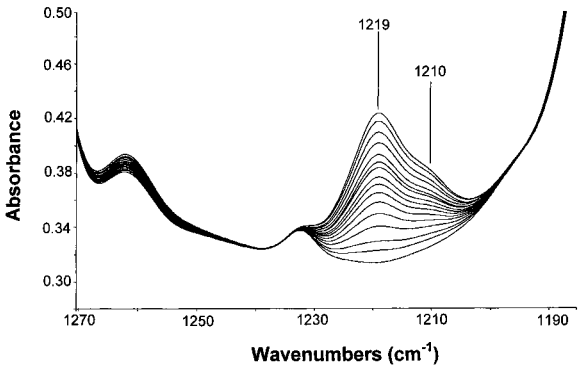

Figure 3. Transmission FTIR spectra in the 1270−1190 cm^{-1} interval collected at different sorption times for the chloroform sorption test at 56 °C and 10 Torr.

The mass transport behavior of this system is quite complex in view of the heterogeneous nature of the polymer (crystalline and amorphous phases) and of the accessibility of the crystalline phase to the penetrant. As a consequence, a detailed description of chloroform transport in a δ-form film of s-PS should be based on a thorough knowledge of polymer morphology and of the trasport properties of the anisotropic crystalline phase, which are actually lacking. Therefore, in the present contribution, only the overall phenomenology of the mass transport behavior is considered. In Figure 4A−D are reported sorption−desorption kinetics, as evaluated spectroscopically, at the various investigated activities.

Sorption and desorption kinetics evaluated spectroscopically compare well with those evaluated by means of the gravimetric method (see Figure 4C): complete match of results points to the reliability of the FTIR method and to the soundness of the assumptions adopted in performing the quantitative analysis of the spectra. The equilibrium sorption data, expressed as g/100 g of dry polymer, are reported in Table 1. The following discussion will be focused only on data gathered spectroscopically.

Desorption kinetics is almost coincident with sorption at the lowest pressure to become slower and slower, as compared to sorption, as the vapor pressure increases. This is a typical feature of Fickian systems whose diffusivity is an increasing function of the penetrant concentration.[29] Consistent with the above results, the sorption rate displays a marked increase with chloroform pressure and, hence, with chloroform concentration in the polymer (see Figure 5). In the case of homogeneous systems characterized by a mutual diffusivity increasing with concentration, the shape of sorption kinetics curve does not depend significantly on the functional form of the diffusion coefficient and is not

Table 1. Sorption Equilibrium Concentration (C_∞) and Diffusivity Constants for Chloroform in Syndiotactic Polystyrene δ Form at 56 °C and at Several Pressures of Vapor

press. [Torr]	C_∞ [g/100 g of dry sample] (absorption)	D [cm²/s] (absorption)	D_1^d [cm²/s] (desorption)	D_2^d [cm²/s] (desorption)	$\bar{D}$ [cm²/s]
5	2.15	$8.6 \times 10^{-13} \pm 7 \times 10^{-15}$	$1.5 \times 10^{-12} \pm 8 \times 10^{-14}$	$9.0 \times 10^{-13} \pm 7 \times 10^{-14}$	$1.2 \times 10^{-12} \pm 9 \times 10^{-14}$
10	4.31	$1.8 \times 10^{-12} \pm 8 \times 10^{-15}$	$1.35 \times 10^{-12} \pm 6 \times 10^{-14}$	$9.6 \times 10^{-13} \pm 5 \times 10^{-14}$	$1.6 \times 10^{-12} \pm 7 \times 10^{-14}$
20	5.65	$3.4 \times 10^{-12} \pm 1 \times 10^{-14}$	$1.8 \times 10^{-12} \pm 1 \times 10^{-14}$	$1.1 \times 10^{-12} \pm 1.0 \times 10^{-14}$	$2.6 \times 10^{-12} \pm 2 \times 10^{-14}$
100	13.97	$1.6 \times 10^{-11} \pm 1.0 \times 10^{-13}$	$6.2 \times 10^{-12} \pm 1 \times 10^{-14}$	$1.3 \times 10^{-12} \pm 1.0 \times 10^{-14}$	$1.1 \times 10^{-11} \pm 1 \times 10^{-13}$

substantially different from the case of constant diffusivity. In close analogy, in the present case sorption kinetics are satisfactorily fitted, at all investigated pressures, by assuming a Fickian behavior with constant mutual diffusivity (D) which is described, in the case of a plane sheet, by the following relationship:

$$\frac{M_t}{M_\infty} = 1 - \frac{8}{\pi^2}\sum_{m=0}^{\infty}\frac{1}{(2m+1)^2}\exp\left[\frac{-D(2m+1)^2\pi^2 t}{L^2}\right] \quad (3)$$

where M_t is the amount of penetrant absorbed at time t, M_∞ is the amount of penetrant absorbed at equilibrium, and L is the thickness of the sheet. The results of curve-fitting analysis of the sorption curves by using eq 3 are compared with the experimental data in Figure 5. It is to be remarked that the diffusivity values determined in this way are actually averages over the ranges of concentration proper of each sorption test.

In analogy to homogeneous Fickian systems characterized by a diffusivity increasing with penetrant concentration, the linear trend of the sorption curve with the square root of time extends up to values of $A_t/A_\infty \equiv M_t/M_\infty$ well above 0.5. The extent of this linear region increases with the chloroform pressure. Consistent with the above observations, the linear behavior in the desorption tests is gradually suppressed as the chloroform pressure increases. The shape of desorption curves is expected to depend significantly on the functional form of the diffusion coefficient when it increases with concentration. Hence, in the case of desorption, a Fickian model based on a constant diffusivity (eq 3) does not provide an accurate description of the kinetic behavior. Therefore, short time (D_1^d) and long time (D_2^d) diffusivity constants have been evaluated by fitting with eq 3 the initial ($M_t/M_\infty < 0.25$) and final ($M_t/M_\infty > 0.75$) parts of the desorption curves. In analogy to homogeneous systems characterized by a concentration-dependent diffusivity, an average value for diffusivity in the appropriate range of concentration of each test could be evaluated from eq 4:[29]

$$\bar{D}(0,C_0) = \frac{1}{C_0}\int_0^{C_0} D(C)\,\mathrm{d}c \cong (D_1^a + D_1^d) \quad (4)$$

where $\bar{D}(0,C_0)$, C_0, D_1^a, and D_1^d represent respectively the average diffusivity in the concentration range $[0,C_0]$, the equilibrium concentration of penetrant at a certain pressure, the short time diffusivity for the absorption test, and the short time diffusivity for the desorption test. Both D_1^a and D_1^d are evaluated for sorption and desorption tests performed between the same pressure values. In the case at hand $D_1^a = D$. On the other hand, the value of D_2^d supplies an estimate of $D(C_0)$ evaluated at $C_0 = 0$.

Short time and long time diffusivities, along with average values calculated by eq 4, are reported in Table 1, where the considerable increase of $\bar{D}(0,C_0)$ can be appreciated (about 1 order of magnitude in passing from 5 to 100 Torr).

3.2. Host−Guest Molecular Interactions. The FTIR-based technique is particularly useful also because of the wealth of information at molecular level present in the vibrational spectrum. This information can be used, for example, for studying the molecular interactions between the penetrant molecules and the polymeric substrate. We have already noted that the δ_{Cl-C-H} peak of chloroform is split in two components when sorbed in the δ-form. This experimental evidence can be accounted for by assuming that, when a chloroform molecule is hosted in the cavities of the nanoporous crystalline phase, specific molecular interactions with the surrounding environment occur, determining detectable changes in the infrared spectrum. Normally, whenever strong molecular interactions are formed, they cause a significant increase of the molar absorptivities of the normal modes involving the centers taking part in the interaction. This is due to the quadratic dependence of the molar absorptivity, ϵ, with the derivative of the dipole moment, μ, with respect to the normal coordinate, Q, of the vibration:

$$\epsilon = \left(\frac{8\pi^2 N_A}{3hc}\right)\nu\left|\frac{\partial\mu}{\partial Q}\right|^2 \quad (5)$$

where N_A is the Avogadro's number, h is Planck's constant, c is the speed of light, and ν is the frequency of the band center.[30]

Therefore, the absolute value of molar absorptivity for suitable normal modes is much more sensitive to the occurrence of molecular interaction than, for instance, the displacement of peak position. The combination of gravimetric and spectroscopic measurements provides the opportunity for an accurate evaluation of ϵ. This is shown in Figure 6A where is reported the reduced absorbance ($A/L = \epsilon C$) of the peak at 1219 cm^{-1} as a function of the chloroform concentration, C, expressed in mol/cm^3. Chloroform concentration has been evaluated by assuming that in the polymer/penetrant mixture partial molar volume of chloroform is zero. This assumption is justified by the fact that the fraction of chloroform hosted in the cavities of the crystalline phase does not contribute any additive volume to the system, while the fraction absorbed in the glassy amorphous phase is likely to be characterized by a negligible partial molar volume.[31] The curves relative to the different pressures display a linear behavior, and the slopes are essentially independent of the test pressure (see Figure 6A). Since the profile of the analytical peak is made of two components, the validity of the Beer−Lambert relationship implies the closeness of the molar absorptivity values for the two components.

The average value of ϵ, as derived from the diagrams at different pressures, is 1.50×10^3 cm mmol^{-1}. This value is to be compared with the molar absorptivity of the same vibration for the isolated molecule (1.54×10^3

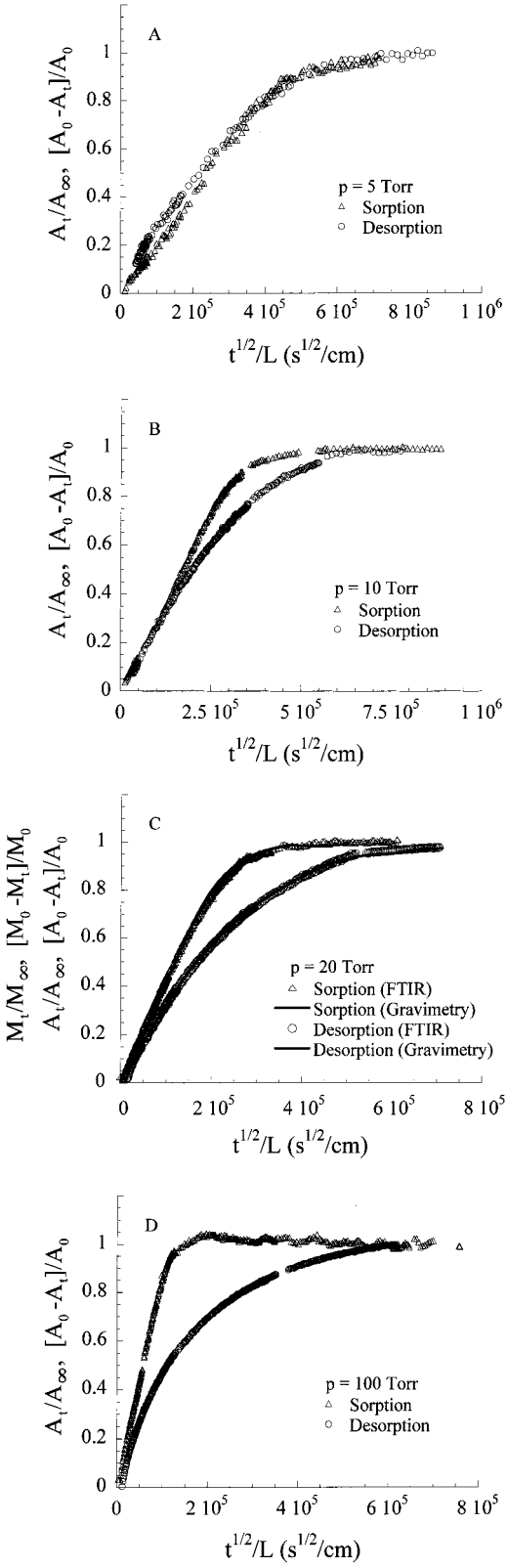

Figure 4. Sorption and desorption kinetics as monitored spectroscopically. Chloroform pressures as indicated. In (C) are also reported, for comparison, the kinetic curves as evaluated gravimetrically (continuous lines).

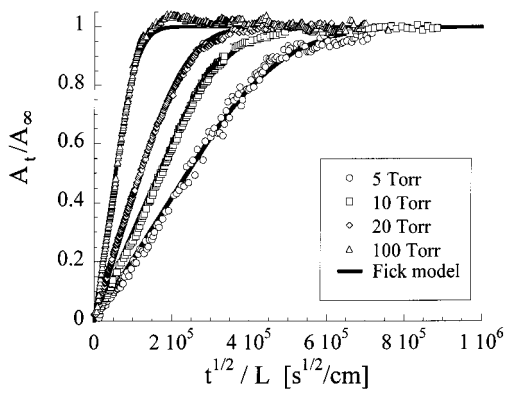

Figure 5. Comparison between the experimental sorption curves and the kinetic profiles calculated by assuming ideal Fickian behavior (continuous lines).

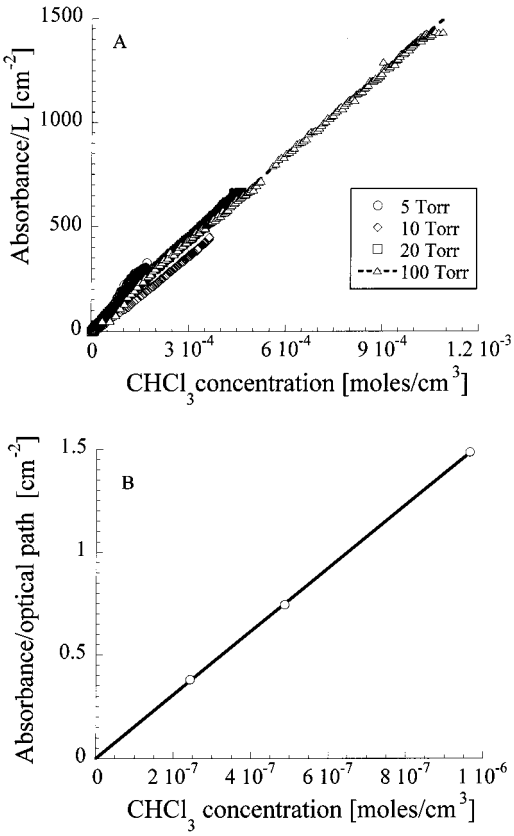

Figure 6. Reduced absorbance of the chloroform band at 1219 cm^{-1} as a function of concentration: (A) chloroform absorbed in s-PS; (B) chloroform vapor at different pressures.

cm $mmol^{-1}$), which has been measured from the vapor phase spectra of choloroform at different pressures (see Figure 6B). In the limits of the experimental uncertainty, the two ϵ values can be considered coincident. This experimental finding implies that the molecular interactions which cause the peak splitting are intrinsically weak and/or that the population of molecules involved in such interaction is relatively small, so that the behavior of the composite profile is mainly controlled by the umperturbed component at higher frequency.

We have observed that the relative contribution of the components at 1220 and 1210 cm^{-1} depends on the test pressure and, hence, on the concentration of chloroform in the sample. For the spectra collected on samples at sorption equilibrium at the different pressures, we separated the composite profile in the two components by means of the curve-resolving algorithm described in the Experimental Section. The results of this analysis are reported in Figure 7A. An interesting feature of this plot is that the 1210 cm^{-1} component attains a plateau level for pressures higher than 20 Torr. This behavior is consistent with the hypothesis that the peak at 1210

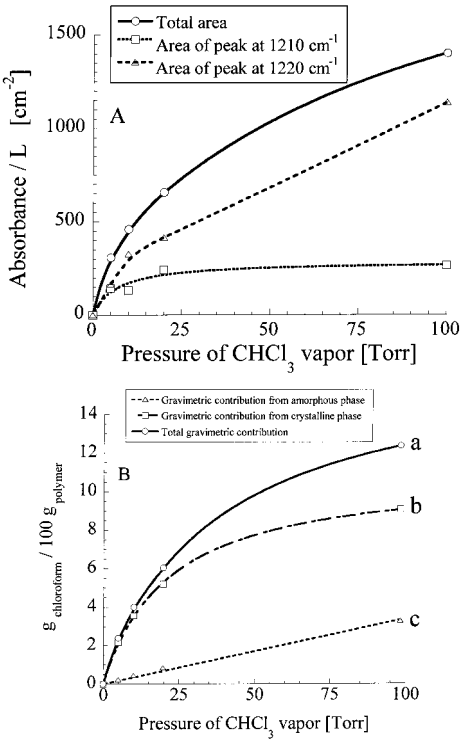

Figure 7. (A) Reduced absorbance of the chloroform peak centered at 1219 cm^{-1} and of the two components at 1220 and 1210 cm^{-1}, as a function of the penetrant pressure. Lines are drawn to guide eye. (B) Sorption isotherms evaluated gravimetrically. Curve a: overall sorption for semicrystalline sample. Curve b: calculated contribution of the crystalline phase. Curve c: calculated contribution of the amorphous phase.

cm^{-1} is related only to molecules hosted in the crystalline cavities, and the plateau reflects attainment of saturation of the adsorption capability of the crystalline phase. The curve relative to the component at 1220 cm^{-1} displays a completely different behavior, characterized by an initial rapid increase up to around 15 Torr, thereafter increasing at a slower rate. This behavior can be ascribed to the fact that this component is contributed by chloroform molecules in both phases. In particular, the contribution of molecules hosted in the crystalline cavities prevails at low pressures and causes the initial steep increase. When saturation of crystal cavities is attained, the absorbance increase is only due to sorption in the amorphous phase, which is characterized by a lower solubility.[17]

The assignment of the 1210 and 1220 cm^{-1} bands respectively to $CHCl_3$ molecules absorbed in the crystalline phase and to molecules absorbed in both the crystalline and amorphous phases is supported by further spectroscopic and gravimetric experimental evidence.

In fact, tests performed on amorphous samples of atactic PS at sorption equilibrium with $CHCl_3$ vapor reveal, as already noted, the presence of the sole component at 1220 cm^{-1}, supporting the conclusion that the 1210 cm^{-1} band present in semicrystalline sPS is contributed only by chloroform molecules absorbed in the crystalline phase.

In Figure 7B are reported equilibrium sorption data evaluated gravimetrically both for atactic PS (amorphous), curve c, and for nanoporous semicrystalline sPS, curve a, in the same temperature and pressure conditions as for the spectroscopic tests. On the basis of these experimental results and of the crystallinity degree of the samples, the contribution of molecules absorbed in each phase has been evaluated. The calculation is based on the assumption that the sorption behavior of the amorphous phase of semicrystalline sPS is identical to that of atactic PS. The contribution of crystalline phase, calculated by difference, is reported in curve b of Figure 7B. It is observed that the equilibrium amount of chloroform absorbed in the amorphous phase increases linearly with pressure, while that of the crystalline phase displays an evident downward concavity, slowly approaching a plateau, as expected in the case of sorption in a nanoporous phase with a limited amount of sorption sites. These results clearly support the proposition that the 1220 cm^{-1} peak is contributed also by a fraction of $CHCl_3$ molecules absorbed in the crystalline domains. In fact, the evident downward concavity in the 1220 cm^{-1} absorbance data reflects the same feature observed for the gravimetric crystalline contribution, which is absent in the gravimetric sorption behavior of the amorphous phase. Thus, the absorbance of the 1220 cm^{-1} peak results from the addition of a linearly increasing component (molecules absorbed in the amorphous phase) and a nonlinearly increasing component which progressively flattens (molecules absorbed in the crystalline phase).

Furthermore, in the spectrum of the sample equilibrated at 5 Torr, where the amount of chloroform absorbed in the amorphous phase is less than 10% of the total (see Figure 7B), the intensity of the 1220 cm^{-1} component is comparable to that of 1210 cm^{-1} peak (see Figure 7A). In view of the closeness of the molar absorptivities of the above peaks, this experimental evidence confirms that the 1220 cm^{-1} component is contributed by chloroform absorbed in both phases, which, in turn, would indicate the existence of two distinct populations of guest molecules in the crystalline phase.

3.3. Structural Changes of the s-PS Crystalline Phase upon Sorption. The infrared spectrum of s-PS is very sensitive to the local conformation of the macromolecules. Bands characteristic of each conformation have been detected and, in particular, TT at 1349, 1224, and 537 cm^{-1}; TTGG at 1354, 1277, 572, and 502 cm^{-1}; TG at 1327, 1197, 1185, 920, 896, 620, 580, 566, and 500 cm^{-1}.[32] Some of these bands are influenced not only by the type of conformation but also by its sequential length, and the sensitivity to the length of a particular conformation differs from band to band. It is possible to introduce the concept of critical sequence length (CSL), which is defined as the shortest length of the sequence of a particular conformation, represented by the number (*m*) of monomeric units contained in the sequence, necessary for the band to appear.[33,34] The bands in the region 600−450 cm^{-1} are due to the out-of-plane deformation of the phenyl ring;[35] they were found to be conformationally sensitive to the TTGG sequence and strongly influenced by its length.

In Figures 8 are reported the spectra of an empty δ form sample (trace A) and of an amorphous s-PS sample (trace B) in the 1420−1225 cm^{-1} range (Figure 8a) and in the 610−470 cm^{-1} interval (Figure 8b). In the low-frequency region, the spectrum of the amorphous sample displays a symmetrical peak at 538 cm^{-1} with broad bands on both sides of the principal component. The spectrum of the empty δ form is considerably different: two sharp peaks appear at 571 and 503 cm^{-1}, and the

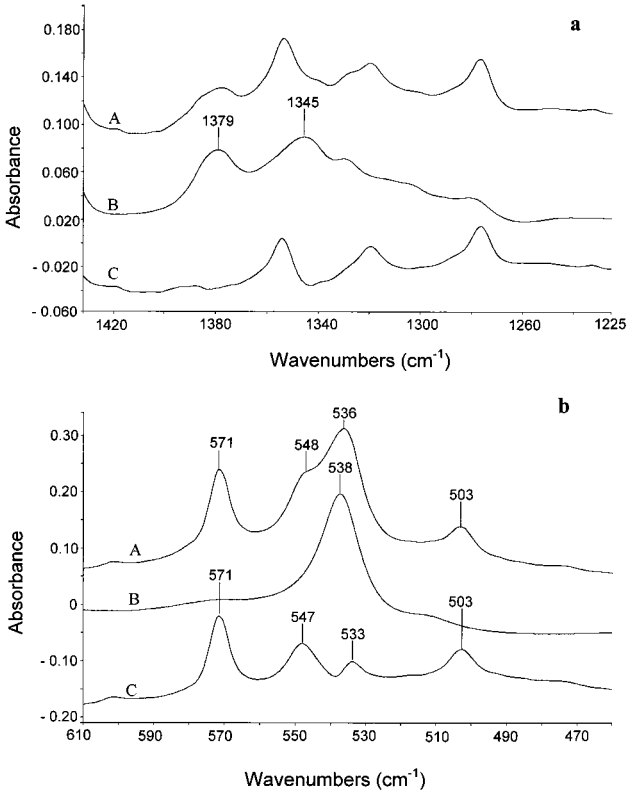

Figure 8. FTIR transmission spectra of s-PS in δ form (trace A), amorphous s-PS (trace B), difference spectrum (A) − (B) (trace C): a, 1420−1225 cm^{-1} range; b, 610−470 cm^{-1} range.

amorphous peak at 538 cm^{-1} is split in two components at 548 and 536 cm^{-1}. Kobayashi et al.[36] suggest that in this region two conformationally sensitive peaks are present at 549 and 536 cm^{-1}, superimposed on the amorphous band at 538 cm^{-1}. By using an isotope dilution technique, Tashiro et al.[37] were able to determine the critical sequence length for the various peaks in this frequency region. Thus, m was estimated to be 20−30 (corresponding to 5−7 turns of the helix) for the peak at 572 cm^{-1}, 7−12 for the 549 cm^{-1} peak, 5−10 for the 536 cm^{-1} peak, and 12−20 for the 502 cm^{-1} peak.

Following an approach developed earlier for the α and β forms of s-PS,[38] we were able to isolate the spectrum of the pure crystalline phase from that of the semicrystalline δ form by subtracting out the contribution of the amorphous phase. In the present case application of difference spectroscopy is not straightforward, owing to the difficulty of identifying well-resolved, purely amorphous peaks. By careful inspection of samples having different degrees of crystallinity, these peaks were identified in the conformationally sensitive region between 1400 and 1300 cm^{-1}, at 1379 and 1345 cm^{-1}. Thus, the spectral subtraction was accomplished by choosing the K parameter (see experimental) so as to reduce both the above bands to the baseline. A typical result of such an analysis is reported in Figure 8a, trace C, for the 1400−1300 cm^{-1} range and in Figure 8b, trace C, for the 610−470 cm^{-1} interval. It is seen that difference spectroscopy affords the complete resolution of the four conformationally sensitive components located below 600 cm^{-1}; these peaks are very relevant to the characterization of the structural ordering of the system since, as already mentioned, each one corresponds to a different sequence length.

As discussed in detail in ref 38, the subtraction factor, K, is quantitatively related to the crystallinity degree

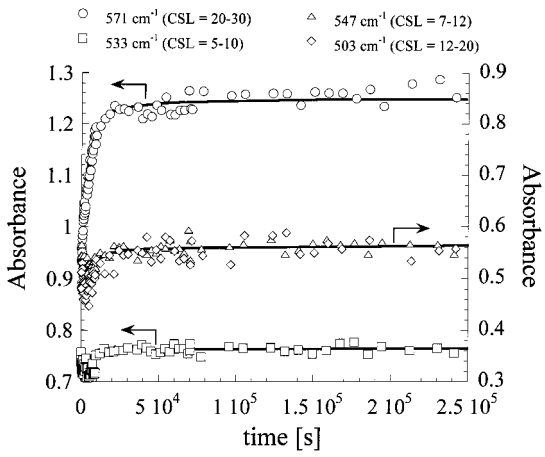

Figure 9. Absorbance of the conformationally sensitive s-PS peaks at 571, 547, 533, and 503 cm^{-1} as a function of time during the cholorform sorption test at 100 Torr. Data relative to the 533 cm^{-1} peak have been arbitrarily shifted along the Y axis to facilitate comparison. Lines are drawn to guide eye.

of the sample, expressed as weight fraction, X_c, according to

$$K = \frac{L}{L'}(1 - X_c) \tag{6}$$

where L and L' are the thickness of the films used to collect the sample and the reference spectra. The ratio L/L' can be estimated spectroscopically from the absorbance ratio of a conformationally insensitive peak (i.e., at 1601 cm^{-1}).

Furthermore, the absorbance value at 571 cm^{-1} allows us to evaluate the weight fraction, x_{571}, of monomeric units located in the ordered TTGG sequences equal or longer than the critical sequence length of the peak (m = 20−30), by use of the equation[36]

$$\frac{1}{x_{572}} = 1 + \left(\frac{\epsilon_{572}}{\epsilon_{540}}\right)\left(\frac{A_{540}}{A_{571}}\right) \tag{7}$$

In the above equation the amorphous contribution, A_{540}, was evaluated by considering the area of the amorphous peak at 540 cm^{-1} which was subtracted to obtain the difference spectrum, while the absorptivity ratio $\epsilon_{540}/\epsilon_{571}$ was taken to be 0.838, according to the evaluation made by Kobayashi et al.[36]

In Figure 9 is reported the absorbance of the peaks at 571, 547, 533, and 503 cm^{-1} as a function of time during the sorption test at a chloroform vapor pressure of 100 Torr. The intensity of all the peaks increase in the early stages of the sorption process, reaching a plateau value after about 2×10^4 s. However, while the 571 cm^{-1} peak increases by 50% of its initial value, only minor changes (less than 20%) are detected in the intensity of the other peaks. The above results indicate that chloroform sorption at 100 Torr induces a structural rearrangement of the δ crystalline form and, in particular, a considerable increase in concentration of the longer helix sequences (20−30 units), while the concentration of the shorter sequencies is only marginally affected.

Figure 10 shows the molar fraction of monomeric units located into helical sequences with at least 20−30 units as a function of time for the sorption and desorption tests at 100 Torr (curves A and B, respectively) and for the sorption test at 20 Torr (curve C).

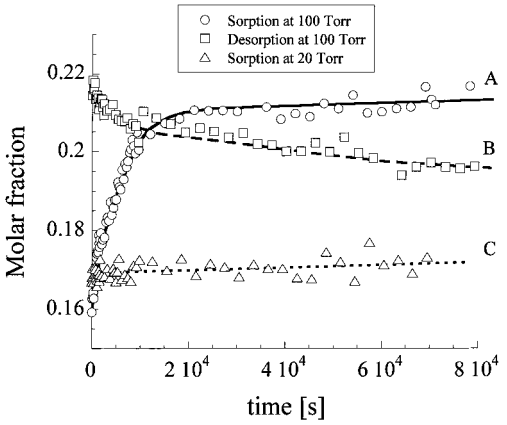

Figure 10. Time evolution of the molar fraction of monomers located into helical sequences with CSL ≥ 20−30. Curve A: sorption test at 100 Torr. Curve B: desorption test at 100 Torr. Curve C: sorption test at 20 Torr. Lines are drawn to guide the eye.

Comparison of curves a and b indicates that the process leading to the structural ordering of the system is not fully reversible. Once the chloroform that has produced the crystallization of s-PS is allowed to escape from the sample, only a limited decrease in concentration of the longer sequences is observed. The curve relative to the test at 20 Torr shows that, in these conditions, no structural rearrangements take place in the sample, thus indicating that, for the recrystallization process to be initiated, it is necessary to reach a critical concentration of chloroform in the sample.

Occurrence of further conformational ordering is expected to take place inside the sample exposed to chloroform vapors, once the penetrant concentration at a specific point reaches, as a consequence of diffusional transport, a critical value above which the enhancement of macromolecular mobility allows conformational rearrangements. At p = 100 Torr, this threshold value is immediately attained in the outer region of the specimen since the equilibrium concentration of chloroform at p = 100 Torr is higher than the critical concentration level. As penetration profiles evolve with time, the fraction of amorphous domains where this threshold value is exceeded increases. On the other hand, at p = 20 Torr, at any time the threshold value is never attained in any point inside the sample, since the equilibrium value is lower than the critical one.

Interesting considerations can also be made by considering the evolution of the crystallinity degree during sorption and desorption processes. In Figure 11 is reported the percent b.w. crystallinity, $100X_c$, as evaluated by eq 6, as a function of time for the sorption and desorption tests at 100 Torr. Also shown, for comparison, is the curve of chloroform concentration vs time, relative to the sorption measurement. The initial crystallinity degree of the δ form is estimated to be 34% and is found to increase up to 39% as a consequence of chloroform sorption. The crystalline structure developed as a consequence of sorption is stable since no detectable changes of X_c are found when chloroform is desorbed. The kinetics of the recrystallization process exactly parallels that of the vapor sorption. In fact, X_c increases steeply when the sorption rate is higher, i.e., in the early stages of the process, while reaching a plateau value when the sorption process terminates.

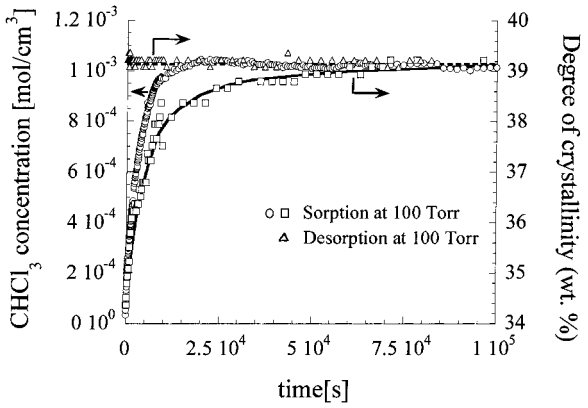

Figure 11. Time evolution of the crystallintiy degree of s-PS during sorption and desorption tests at 100 Torr. Also shown, for comparison, is the chloroform concentration vs time curve relative to the sorption test. Lines are drawn to guide the eye.

4. Conclusions

The transport of chloroform vapor in films of nanoporous semicrystalline s-PS has been investigated by time-resolved FTIR spectroscopy and by gravimetric analysis. Fickian behavior has been observed, and apparent diffusivities increase significantly with concentration. Accordingly, sorption rate has been found to be faster than desorption, with the difference becoming larger and larger as the vapor activity increases. In the present contribution we have considered the overall transport behavior. Details related to the heterogeneous structure of the material (amorphous and nanoporous crystalline phases) will be dealt with in a forthcoming investigation.

The spectroscopic analysis has shown that, when chloroform is absorbed in the crystalline phase, a significant perturbation of its vibrational spectrum takes place which is not observed in the case sorption in the amorphous phase. This effect is likely to be related to host−guest molecular interactions. A quantitative evaluation of the absorptivity of a chloroform peak has, however, demonstrated that these interactions are intrinsically weak. The perturbation of the infrared spectrum may allow to discriminate between chloroform molecules absorbed into the amorphous and crystalline phases. Preliminary results along this direction indicate that saturation of the crystalline sorption capacity occurs around a vapor pressure of 20 Torr at 56 °C. The spectroscopic analysis has also revealed that sorption of chloroform induces conformational rearrangements of the semicrystalline s-PS, leading to an increase of δ form crystallinity (from 34 to 39% at a vapor pressure of 100 Torr). This effect is not reversible upon desorption of chloroform. It has also been possible to follow the time evolution of several helical sequences, characterized by different number of monomeric units. The experimental results suggest that the conformational rearrangement induced by chloroform sorption leads preferentially to an increase of the longer and more structurally regular sequences.

The experimental approach developed in the present contribution demonstrates the possibility of monitoring concurrently the mass transport and the related structural modifications occurring in the polymeric substrate. This methodology supplies an important tool to correlate the two processes in view of improving our fundamental understanding of their mutual interplay.

References and Notes

(1) Chatani, Y.; Fuji, Y.; Shimane, Y.; Ijitsu, T. *Polym. Prepr. Jpn. (Engl. Ed.)* **1988**, *37*, E428.
(2) Immirzi, A.; de Candia, F.; Iannelli, P.; Vittoria, V.; Zambelli, A. *Makromol. Chem., Rapid Commun.* **1988**, *9*, 761.
(3) Guerra, G.; Vitagliano, V. M.; De Rosa, C.; Petraccone, V.; Corradini, P. *Macromolecules* **1990**, *23*, 1539.
(4) Guerra, G.; Musto, P.; Karasz, F. E.; MacKnight, W. J. *Makromol. Chem.* **1990**, *191*, 2111.
(5) Greis, O.; Xu, Y.; Asano, T.; Petermann, J. *Polymer* **1989**, *30*, 90.
(6) De Rosa, C.; Guerra, G.; Petraccone, V.; Corradini, P. *Polym. J.* **1991**, *23*, 1435.
(7) Cartier, L.; Okihara, T.; Lotz, B. *Macromolecules* **1998**, *31*, 3303.
(8) De Rosa, C.; Rapacciuolo, M; Guerra, G.; Petraccone, V.; Corradini, P. *Polymer* **1992**, *33*, 1423.
(9) De Rosa, C.; Guerra, G.; Petraccone, V.; Pirozzi, B. *Macromolecules* **1997**, *30*, 4147.
(10) Chatani, Y.; Shimane, Y.; Inagaki, T.; Ijitsu, T.; Yukinari, T.; Shikuma, H. *Polymer* **1993**, *34*, 1620.
(11) Chatani, Y.; Inagaki, T.; Shimane, Y.; Shikuma, H. *Polymer* **1993**, *34*, 4841.
(12) De Rosa, C.; Rizzo, P.; Ruiz de Ballesteros, O.; Petraccone, V.; Guerra, G. *Polymer* **1999**, *40*, 2103.
(13) Rapacciuolo, M.; De Rosa, C.; Guerra, G.; Mensitieri, G.; Apicella, A.; Del Nobile, M. A. *J. Mater. Sci., Lett.* **1991**, *10*, 1084.
(14) Guerra, G.; Manfredi, C.; Rapacciuolo, M.; Corradini, P.; Mensitieri, G.; Del Nobile, M. A. Italian Patent 1994 (CNR).
(15) Reverchon, E.; Guerra, G.; Venditto, V. *J. Appl. Polym. Sci.* **1999**, *74*, 2077.
(16) Milano, G.; Venditto, V.; Guerra, G.;.Cavallo, L.; Ciambelli, P.; Sannino, D. *Chem. Mater.*, in press.
(17) Manfredi, C.; Del Nobile, M. A.; Mensitieri, G.; Guerra, G.; Rapacciuolo, M. *J. Polym. Sci., Polym. Phys. Ed.* **1997**, *35*, 133.
(18) Guerra, G.; Milano, G.; Venditto, V.; Musto, P.; De Rosa, C.; Cavallo, L. *Chem. Mater.* **2000**, *12*, 363.
(19) Michaels, A. S.; Bixler, H. J. *J. Polym. Sci.* **1961**, *50*, 393.
(20) Puleo, A. C.; Paul, D. R.; Wong, P. K. *Polymer* **1989**, *30*, 1357.
(21) Muller-Plathe, F. *J. Chem. Phys.* **1995**, *103*, 4346.
(22) Musto, P.; Manzari, M.; Guerra, G. *Macromolecules* **1999**, *32*, 2770.
(23) Musto, P.; Manzari, M.; Guerra, G. *Macromolecules* **2000**, *33*, 143.
(24) Cotugno, S.; Larobina, D.; Mensitieri, G.; Musto, P.; Ragosta, G. *Polymer* **2001**, *42*, 6431.
(25) Zambelli, A.; Longo, P.; Pellecchia, C.; Grassi, A. *Macromolecules* **1987**, *20*, 2035.
(26) Koenig, J. L. *Spectroscopy of Polymers*; ACS Professional Ref. Books; American Chemical Society; Washington, DC, 1992; pp 56−61.
(27) Krishnan, K.; Ferraro, J. R. In *Fourier Transform Infrared Spectroscopy*; Ferraro, J. R., Basile, L. J., Eds.; Academic: New York, 1982; Vol. 3, p 198.
(28) Marquardt, D. W. *J. Soc. Ind. Appl. Math.* **1963**, *11*, 441.
(29) Crank, J. *The Mathematics of Diffusion*, 2nd ed.; Clarendon Press: Oxford, 1975.
(30) Gribov, L. A. *Intensity Theory for Infrared Spectra of Polyatomic Molecules*; Consultants Bureau: New York, 1964.
(31) Fleming, G. K.; Koros, W. J. *Macromolecules* **1990**, *23*, 1353.
(32) Kobayashi, M.; Nakaoki, T.; Ishihara, N. *Macromolecules* **1990**, *23*, 78.
(33) Kobayashi, M.; Akita, K.; Tadokoro, H. *Makromol. Chem.* **1968**, *113*, 324.
(34) Kobayashi, M.; Tsumura, K.; Tadokoro, H. *J. Polym. Sci., Polym. Phys. Ed.* **1968**, *6*, 1493.
(35) Liang, C.Y.; Krimm, S. *J. Polym. Sci.* **1958**, *27*, 241.
(36) Kobayashi, M.; Yoshioka, T.; Imai, M.; Itoh, Y. *Macromolecules* **1995**, *28*, 7376.
(37) Tashiro, K.; Ueno, Y.; Yoshioka, A.; Kobayashi, M. *Macromolecules* **2001**, *34*, 310.
(38) Musto, P.; Tavone, S.; Guerra, G.; De Rosa, C. *J. Polym. Sci., Polym. Phys. Ed.* **1997**, *35*, 1055.

MA011684D